Comparison of Fault-Location Techniques for Submarine Export Cables in Offshore Wind Farms

Adrian W. Diaz Sarmiento, Jaimis S. L. Colqui, Jose Pissolato Filho, and F. B. Costa

***Abstract*—This paper evaluates the performance of phasor-based and traveling-wave fault-location techniques for submarine export cables in offshore wind farms that utilize grid-following Type-4 inverter-based resources (IBRs). A detailed electromagnetic transient (EMT) model of the Horns Rev 2 offshore wind farm is used to evaluate four phasor-based techniques (impedance-based, simple reactance, Takagi, and modified Takagi) and two traveling-wave techniques (single-ended and double-ended). Among the phasor-based methods, the simple reactance and modified Takagi approaches provide the most consistent estimates, although both require approximately 50–60 ms for transient stabilization. In contrast, the single-ended and double-ended traveling-wave methods achieve the highest location accuracy, supported by transformer stray capacitances that preserve high-frequency wavefronts at the IBR side. The results offer guidance for selecting reliable fault-location techniques for offshore wind export cable protection and monitoring.**

***Index Terms*—Fault Location, Traveling waves, Submarine cables, Offshore Wind farm, Grid-following.**

I. Introduction

The expansion of offshore wind farms (OWFs) has led to increasingly large projects located farther from shore to harness stronger and more stable wind resources. These installations rely on long high-voltage AC (HVAC) submarine export cables to transfer power from the offshore collection system to the onshore grid. As a result, submarine export cables have become critical components of modern transmission infrastructure, exhibiting electrical and operational characteristics that differ significantly from those of conventional onshore systems [1].

Faults in submarine cables are particularly severe, often causing permanent insulation damage that necessitates costly and time-consuming offshore repairs. Therefore, fast detection and accurate fault location are essential to reduce downtime and ensure OWF availability [2]. Traditional diagnostic techniques such as time-domain reflectometry (TDR) and bridge methods [3], [4] can locate faults but require external test equipment and do not provide continuous online monitoring.

Accurate online fault location is challenging because submarine cables exhibit higher capacitance, stronger frequency-dependent attenuation, and sheath–armour electromagnetic coupling, which challenge both transient and phasor-based fault-location accuracy [5]. These difficulties are further amplified in OWFs dominated by grid-following Type-4 inverter-based resources (IBRs), where fault current is shaped by control dynamics rather than electromechanical system response. As a result, the apparent impedance no longer reflects the physical line impedance, reducing the reliability of distance-based estimation [6].

Traveling-wave (TW) methods address these limitations by exploiting the arrival times of high-frequency transients and can provide faster, more accurate fault location [7]. However, such approaches often require high sampling rates and, in double-ended configurations, precise time synchronization between terminals, which increases implementation complexity [8].

In order to provide a performance assessment under realistic offshore conditions, this paper presents a comparative evaluation of phasor- and traveling-wave-based fault-location techniques applied to the submarine export cables of the Horns Rev2 OWF [9]. The analysis focuses on the influence of fault resistance, location, and inception angle on the accuracy, robustness, and response time of each method, aiming to identify the most suitable approaches for offshore applications. Among the phasor-based methods evaluated, the Simple Reactance Method and the Modified Takagi Method provided the most accurate fault-location estimates; however, both required approximately 50 ms of post-fault transient decay before a stable result could be obtained. In contrast, the single-ended and double-ended traveling-wave methods delivered reliable fault-location results without requiring a stabilization period.

II. Phasor-Based Fault Location techniques

This work examines state-of-the-art single-ended fault-location methods [10], which estimate the fault position from voltage and current phasors measured at the offshore wind-farm busbar.

A. Impedance-Based Method (IMBM)

The impedance-based fault location method estimates the distance to the fault using voltage and current measurements obtained from a single terminal of the line [11]. The voltage drop from the sending end can be expressed as:

$$V_{\mathrm{S}} = m\, Z_{1\mathrm{L}}\, I_{\mathrm{S}} + R_{\mathrm{F}}\, I_{\mathrm{F}} \qquad (1)$$

For a single-phase-to-ground fault in phase A, the sending-end voltage and current are defined as $V_{\mathrm{S}} = V_{a\text{-}g}$ and $I_{\mathrm{S}} =$

Adrian W. Diaz Sarmiento, Jaimis S. L. Colqui and José Pissolato are with the Department of Electrical and Computer Engineering, State University of Campinas, Campinas 13083-852, Brazil (e-mail: a196151@dac.unicamp.br, jaimis@unicamp.br, pisso@unicamp.br). F. B. Costa is with the Department of Electrical and Computer Engineering, Michigan Technological University, Houghton, United States of America (e-mail: fbcosta@mtu.edu)

979-8-3315-8138-1

$I_a + k \cdot 3I_0$, where the coefficient k accounts for the mutual coupling between sequence networks and is given by $k = \frac{Z_{1L} - Z_{0L}}{3Z_{1L}}$. The apparent impedance seen from the relay is calculated as $Z_{\text{app}} = \frac{V_S}{I_S}$. Finally, the fault location index m_{LF} is obtained by comparing the apparent impedance with the positive-sequence line impedance:

$$m_{LF} = \text{Re}\left(\frac{Z_{\text{app}}}{Z_{1\text{L}}}\right) \tag{2}$$

B. Simple Reactance Method (SRM)

The simple reactance method is a similar version of the IMBM, where only the reactive component of the apparent impedance is used to estimate the fault location [11]. Neglecting the effect of the fault resistance term $R_F I_F$ in (1), the fault distance can be directly obtained as:

$$m_{LF} = \frac{\text{Im}(Z_{\text{app}})}{\text{Im}(Z_{1\text{L}})} \tag{3}$$

C. Takagi Method (TAKM)

The Takagi approach utilizes both pre-fault and fault measurements. It enhances the accuracy of the simple reactance method [12] by compensating for the influence of load current and reducing the effect of fault resistance. The method employs an incremental current ΔI_S, calculated using the pre-fault current as $\Delta I_S = I_S - I_{\text{pre}}$.

The distance-to-fault m_{LF} is expressed as:

$$m_{LF} = \frac{\text{Im}(V_S\, \Delta I_S^*)}{\text{Im}(Z_{1\text{L}}\, I_S\, \Delta I_S^*)} \tag{4}$$

D. Modified Takagi Method (MTAKM)

The Modified Takagi Method (MTAKM) eliminates the need for incremental quantities. Therefore, it does not require pre-fault data [11]. The distance to the fault m_{LF} can be expressed as:

$$m_{LF} = \frac{\text{Im}\left(V_S\,(3I_0)e^{-jT}\right)}{\text{Im}\left(Z_{1\text{L}}\, I_S\,(3I_0)e^{-jT}\right)} \tag{5}$$

Where, $3I_0$ denotes the measured zero-sequence current, and T represents the angle selected to align the phasors for a specific fault location along the line. The exponential term e^{-jT} provides a phase shift that compensates for system operating conditions and improves fault-location estimation. However, the validity of the selected angle T corresponds to a single fault location, as explained in [11].

III. Traveling-Wave-Based Fault Location Techniques

The fault location is obtained from the arrival times of the incident and reflected traveling waves (TW). For this paper, the filter considered for extraction is the Differentiator–Smoother (DS) filter [13]. The filter output converts the step-like transients into triangular pulses, preserving their amplitude and polarity for accurate time detection.

A. Single-Ended TW Method (SETWM)

This method relies solely on local measurements at the sending terminal [14]. Let t_{11} denote the arrival time of the first incident traveling wave, and t_{13} the arrival time of the first reflected traveling wave at the same terminal. The fault location d can be determined as:

$$d = \frac{v}{2}\,(t_{13} - t_{11}) \tag{6}$$

where v represents the propagation velocity in the cable. Although straightforward to implement, this method requires clear, distinguishable detection of the reflected wave to ensure accurate fault location.

B. Double-Ended TW Method (DETWM)

In the double-ended scheme, incident waves are detected at both terminals [14]. Let t_{11} and t_{21} denote the arrival times of the first incident waves at the local and remote ends, respectively, and L the total line length. The fault distance from the local terminal is given by:

$$d = \frac{1}{2}\,[L - v\,(t_{21} - t_{11})] \tag{7}$$

Compared with the single-ended approach, this method achieves higher accuracy but requires communication and time synchronization between terminals.

IV. Test System Description

The system shown in Fig. 1, based on [9], represents the Horns Rev 2 offshore wind farm connected to the Danish grid through a hybrid transmission link consisting of submarine and underground cables. The offshore wind farm is modeled using a generic grid-following control [15] of a Type-4 configuration. It consists of 91 turbines with a total rated power of 215 MW. The farm is connected to a 220 MVA, 35/35/165 kV three-winding transformer and to a 42 km HVAC submarine export cable, followed by 2.3 km and 55.4 km underground cables. Due to the significant reactive power generated by the long cable sections, a shunt reactor of 80 MVAr is installed between the two underground cables. Two additional shunt reactors (80 MVAr and 40 MVAr) are placed at the Endrup onshore substation. The bulk power system, represented by a three-phase voltage source, is connected to Endrup through a 400 MVA, 167.6/410 kV autotransformer. In the simulation, the generator rating is scaled to 5.2 MVA, representing an equivalent aggregation of 46 identical wind-farm systems.

Table I lists the wind-farm control parameters. The HV export cable is a submarine pipe-type with grounded sheaths and pipe at both ends. The 2.3 km underground cable comprises three cross-bonded, grounded sections. The 55.4 km underground cable has 11 major sections, each with three cross-bonded minor sections, grounded at both ends. Transformer stray capacitances for TW analysis are in Table II. Current is measured via current transformers using the Jiles–Atherton model [16], and voltage via coupling voltage transformers [17]. Sampling rates are 1 MHz for traveling

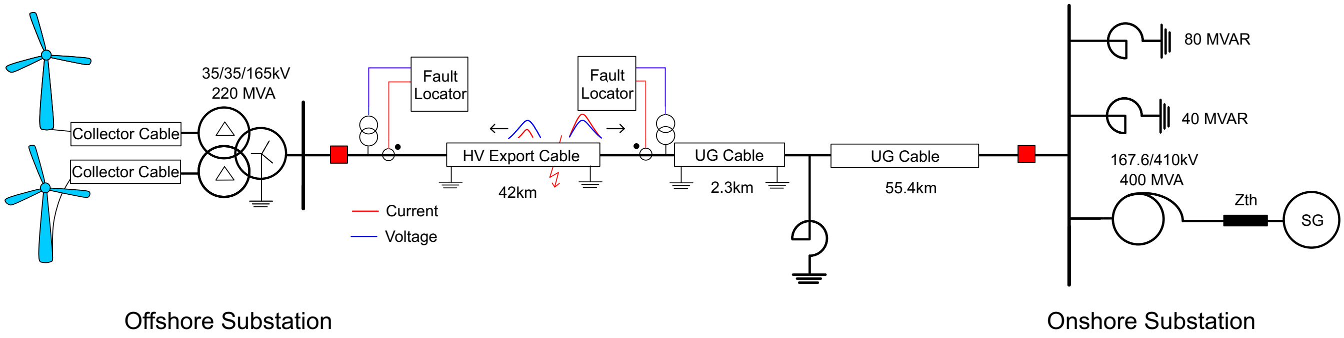

Fig. 1. Offshore wind farm system connected through a submarine cable

TABLE I
WIND TURBINE SPECIFICATIONS.

Component	Modelling parameters
Permanent Magnet Synchronous Generator (PMSG)	5.2 MVA, 0.69 kV, 30 Hz
AC–DC–AC converter	2-level, 3-phase, IGBT-based Switching model
DC link chopper	6 MW, $V_{\text{activation}} = 1.01$ p.u.
Filter with phase reactor	$L_{\text{conv}} = 200\ \mu$H, $C_{\text{filt}} = 1000\ \mu$F $L_{\text{damp}} = 1\ \mu$H, $C_{\text{damp}} = 500\ \mu$F, $R_{\text{damp}} = 1.02\ \Omega$
WT Transformer	5.8 MVA, 0.69/33 kV, 50 Hz, $X_l = 0.08$ p.u.

waves and 3.2 kHz (64 samples/cycle) for phasors. Phasors are computed using a fast Fourier transform with 31 harmonics and an anti-aliasing filter.

TABLE II
STRAY CAPACITANCES OF THE THREE-WINDING TRANSFORMER

Parameter	Value (nF)
C_H	2.4
C_L	7.0
C_T	7.0
C_{HL}	6.0
C_{HT}	6.0
C_{LT}	6.0
C_{busbar}	7.0

V. FAULT LOCATION ANALYSIS IN WIND FARMS

A. Phasor-based methods

All the faults considered in this section are single-line-to-ground faults SLG) applied on phase A at the midpoint of the submarine cable. The fault resistance is varied from 1 to 20 Ω, and the corresponding apparent impedance (Z_{AP}) is shown in Fig. 2, along with the operating zones of a traditional distance relay, to illustrate the impact of fault resistance. As the fault resistance increases, Z_{AP} shifts toward higher resistive values, indicating a strong sensitivity of the estimated impedance to the fault resistance. The reactive component, however, is much less affected, as all trajectories converge to nearly the same value along the imaginary axis. In this case, the resistive reach is limited to $30\,\Omega$, so Z_{AP} remains outside the relay operating zone when the fault resistance exceeds this limit, resulting in a failure of the low-resistance-reach distance element to detect the fault.

Using the fault-location methods described in Section II, the estimated fault locations are shown in Figs. 3 and 4. Fig. 3 shows that the IMBM is highly sensitive to fault resistance. For $R = 1\,\Omega$, the estimated location is $m_{FL} = 0.5253$, which is close to the actual value of 0.5. However, for $R = 5$, 10,

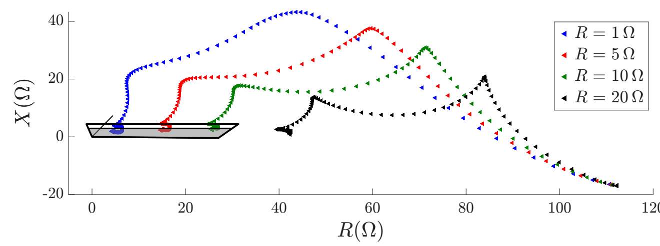

Fig. 2. Apparent impedance calculated at the onshore substation.

and $20\,\Omega$, the method yields $m_{FL} > 1$, resulting in incorrect fault-location estimates. This occurs because the IMBM does not account for the resistive voltage drop across the fault, and because the contribution of current from the grid side dominates the apparent impedance seen at the relay.

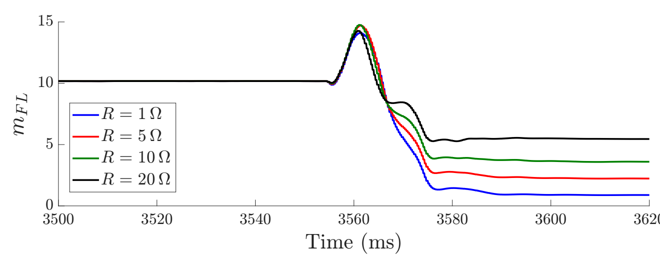

Fig. 3. Fault location using IMBM

Conversely, Fig. 4 shows that the SRM is less affected by the fault resistance. After a transient period of approximately 50 to 60 ms, the steady-state estimates converge to values closer to the true location: $m_{FL} = 0.499$, 0.6153, 0.677, and 0.6257 for $R = 1$, 5, 10, and $20\,\Omega$, respectively. Since the SRM relies primarily on the reactive component, which remains relatively stable under varying fault resistance, it provides more reliable fault-location performance for submarine cables connected to grid-following wind farms, although some deviation persists at high fault resistance.

Fig. 5 presents the reactance calculation during the fault, which is consistent with the results shown in Fig. 4.

979-8-3315-8138-1

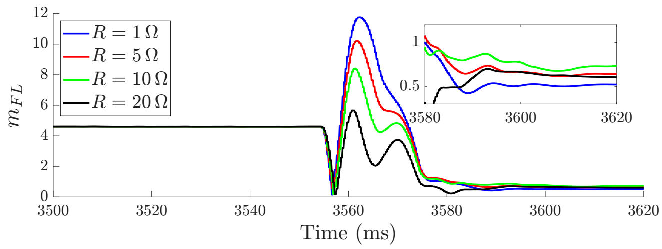

Fig. 4. Fault location using SRM

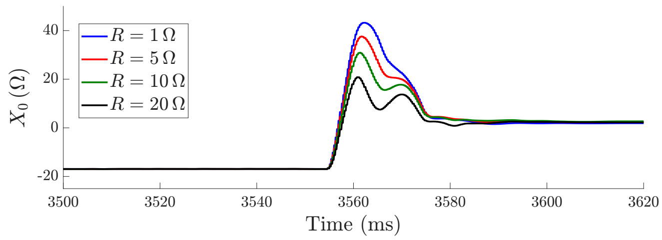

Fig. 5. Reactance calculation during faults

Fig. 6 depicts the calculation when the TAKM is used. This method is severely affected when considering the fault resistance in the simulations. It is shown that for the $R = 1\,\Omega$, the method calculates the fault for $m_{FL} = 0.752$. For the other cases, the TAKM fails to calculate the fault location since m_{FL} exceeds the value of 1, which demonstrates how the Takagi method is also significantly impacted by the fault resistance.

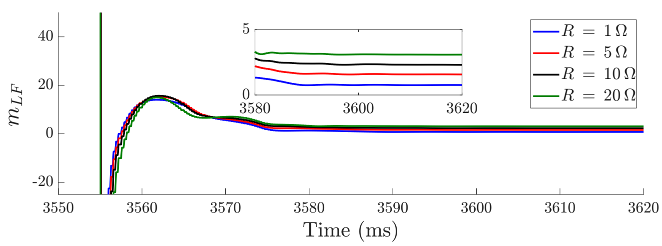

Fig. 6. Fault Location using TAKM

Fig. 7 shows the results obtained using the MTAKM. In this case, an angle $T = 15°$ is considered. Compared to TAKM, this method achieves better results. However, it is still affected by the fault resistance. For a fault resistance of $R = 1\,\Omega$, the estimated location is $m_{FL} = 0.561$. For $R = 5$, 10, and $20\,\Omega$, the values are $m_{FL} = 0.77$, 0.838, and 0.562, respectively. Although the inclusion of the angle T in (5) improves the TAKM performance, this angle is selected assuming a fixed fault angle current T. Therefore, the actual optimal angle T should vary depending on both the fault location and the fault resistance. However, this angle cannot be determined in advance [11].

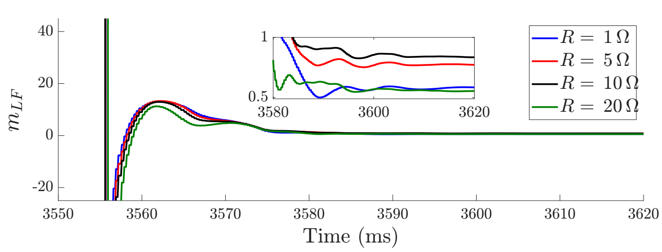

Fig. 7. Fault location using MTAKM

B. TW based methods

A phase-A SLG fault at the cable midpoint was simulated with $R = 1\ \Omega$. Fig. 8 illustrates the resulting fault currents at both terminals of the submarine cable. A high sampling frequency of 1 MHz was utilized to capture the high-frequency transients associated with the arriving TWs. This sampling rate is compatible with the bandwidth of modern current transformers and is already supported by commercially available time-domain relays [13]. To isolate these TWs, a DS filter was applied to the current signals, followed by a simple thresholding technique to precisely determine the TW arrival time at each terminal.

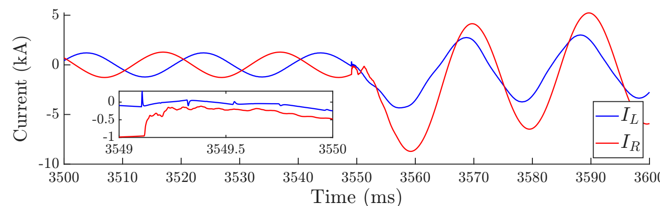

Fig. 8. Phase-A-to-ground fault at mid of the export cable

Fig. 9 shows the phase-A current I_L (blue) and the corresponding DS-filtered signal TW_{IL} (red) measured at the local terminal. The DS-filtered signal clearly reveals the TW arrivals, indicating that the transformer stray capacitances preserve the high-frequency components required for TW detection [18]. The first TW arrival is detected at 3549.107 ms, and the first reflection is at 3549.319 ms. Considering a propagation velocity of 200,000 km/s, the SETWM estimates the fault location at 21.2 km, corresponding to $m_{LF} = 0.5048$.

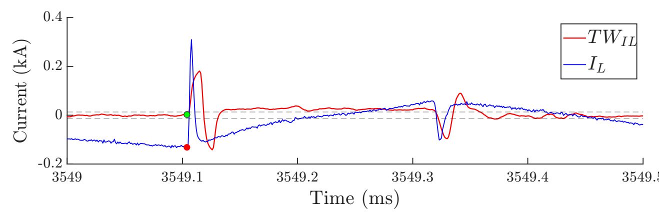

Fig. 9. TWs measured from the IBR side

Similarly, Fig. 10 shows the phase-A current measured at the remote terminal. Although the waveform is more attenuated due to the attenuation of the long submarine cable, the DS-filtered signal still exhibits a clear peak that exceeds the detection threshold, enabling the reliable identification of the first TW arrival at 3549.108 ms. Using the DETWM, the fault is located at 20.9 km, corresponding to $m_{LF} = 0.4976$. In this case, the DETWM provides slightly better accuracy than the SETWM, with a difference of approximately 100 m.

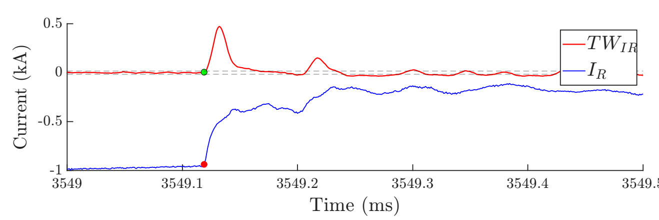

Fig. 10. TWs measured from the grid side

979-8-3315-8138-1

C. Comparison of methods

This section presents the percentage error used to compare the different methods under variations in fault resistance, fault location, and fault inception angle. Table III shows that fault resistance significantly affects phasor-based fault location methods. Among these, the SRM and MTKM yield the most accurate estimates. However, the SETWM and DETWM clearly outperform all phasor-based approaches, achieving superior precision through transient analysis at the μs scale.

Tables IV and V also show that the SRM and MTKM are the most accurate single-ended phasor-based techniques. In contrast, the SETWM and DETWM provide the most reliable fault-location performance overall, except for cases where the fault inception angle is 0°, where their accuracy is highly reduced. The choice of phasor calculation methods and sampling frequency may alter results only during the transient, not in the steady state during the fault, so the results can be regarded as representative of standard impedance-based fault location performance.

TABLE III
PERFORMANCE FOR DIFFERENT FAULT RESISTANCES IN [%]

Resistance [Ω]	IMBM	SRM	TAKM	MTAKM	SETWM	DETWM
1	38	2.53	25.2	6.1	0.48	0.24
5	173	12	108	27	0.48	0.24
10	308	13	181	34	0.48	0.24
20	496	18	259	6	0.48	0.24

TABLE IV
PERFORMANCE FOR DIFFERENT FAULT INCEPTION ANGLES IN [%]

Angle	IMBM	SRM	TAKM	MTAKM	SETWM	DETWM
0°	37	2.53	28.3	6.8	2.62	0.714
30°	39.2	3.33	25.2	6.1	0.48	0.24
45°	34.3	2.85	25.2	6.3	0.48	0.24
60°	32.7	2.53	25.6	6.1	0.48	0.24
90°	38	2.53	25.2	6.2	0.48	0.24

TABLE V
PERFORMANCE FOR DIFFERENT FAULT LOCATION IN [%]

Location [%]	IMBM	SRM	TAKM	MTAKM	SETWM	DETWM
10	38	2.1	25.7	6.1	0.48	0.24
30	38	2.11	24.5	7.3	0.48	0.24
50	42	2.53	25.6	7.2	0.48	0.24
80	44	4.14	27.3	7.9	0.714	0.24
90	49.5	5.7	27.1	8.3	0.714	0.48

VI. CONCLUSIONS

This paper presented a performance assessment of fault-location techniques based on impedance and traveling-wave principles for submarine export cables connecting Type-4 GFL offshore wind farms. Among the impedance-based approaches, the Simple Reactance Method and the Modified Takagi Method exhibited the best overall accuracy. However, both are susceptible to transient settling times of 50–60 ms, driven by the dynamic response of GFL IBRs. If a fault is cleared before stabilization, location errors can exceed 100%. In contrast, the traveling-wave-based techniques (SETWM and DETWM) demonstrated superior accuracy and robustness. Their reliability was maintained under different fault conditions, supported by stray capacitances on the IBR-side transformers that enable detection of the first wavefront arrivals at the offshore terminal.

ACKNOWLEDGMENTS

This work was partially supported by the São Paulo Research Foundation (FAPESP) under Grants 2021/11258-5, 2021/06157-5, 2023/15636-0, and by the National Science Foundation (NSF) under Grant No. 2501861.

REFERENCES

[1] M. Bawart, M. Marzinotto, and G. Mazzanti, "A deeper insight into fault location on long submarine power cables," *CIGRÉ Technical Paper*, 2014.

[2] B. GmbH, "Expert fault location for submarine and underground cables," Tech. Rep., 2020.

[3] G.-Y. Kwon, C.-K. Lee, G. S. Lee, Y. H. Lee, S. J. Chang, C.-K. Jung, J.-W. Kang, and Y.-J. Shin, "Offline fault localization technique on hvdc submarine cable via time–frequency domain reflectometry," *IEEE Transactions on Power Delivery*, vol. 32, no. 3, pp. 1626–1635, 2017.

[4] M. Bawart, M. Marzinotto, and G. Mazzanti, "Diagnosis and location of faults in submarine power cables," *IEEE Electrical Insulation Magazine*, vol. 32, no. 4, pp. 24–37, 2016.

[5] A. Tsylin, A. Graumann Moser, and Z. Gajić, "Relay protection for offshore export cables, challenges and solutions," in *CIGRÉ NRCC Symposium*. Trondheim, Norway: Study Committee B5 – Protection and Automation, 2025, paper No. 1245.

[6] C. Shen and M. Kezunovic, "The impact of control modes of inverter-based resources on distance protection performance," in *2021 IEEE Power & Energy Society General Meeting (PESGM)*, 2021, pp. 1–5.

[7] S. Ghosh, "Testing and validation of travelling-wave-based fault location for submarine cables," *Electric Power Systems Research*, 2023.

[8] S. Xiao, J. Li, and Y. Zhao, "Fault detection and isolation methods in subsea cables," *Sensors*, vol. 20, no. 18, p. 5273, 2020.

[9] C. F. Jensen, *Online location of faults on AC cables in underground transmission systems*. Springer Science & Business Media, 2014.

[10] M. Davi, A. Júnior, C. Grilo, T. Cunha, L. Lessa, M. Oleskovicz, and D. Coury, "An improved methodology to locate faults in onshore wind farm collector systems," *Energies*, vol. 18, no. 3, p. 693, 2025.

[11] K. Zimmerman and D. Costello, "Impedance-based fault location experience," in *2006 IEEE rural electric power conference*. IEEE, 2006, pp. 1–16.

[12] T. Takagi, Y. Yamakoshi, M. Yamaura, R. Kondow, and T. Matsushima, "Development of a new type fault locator using the one-terminal voltage and current data," *IEEE Transactions on Power apparatus and systems*, no. 8, pp. 2892–2898, 2007.

[13] E. P. A. Ribeiro, F. V. Lopes, J. P. G. Ribeiro, and E. J. S. Leite, "Atp/models differentiator-smoother filter model validated using actual time-domain relay," in *2018 Workshop on Communication Networks and Power Systems (WCNPS)*, 2018, pp. 1–4.

[14] P. Gale, P. Crossley, X. Bingyin, G. Yaozhong, B. Cory, and J. Barker, "Fault location based on travelling waves," in *1993 Fifth international conference on developments in power system protection*. IET, 1993, pp. 54–59.

[15] K. Clark, N. W. Miller, and J. J. Sanchez-Gasca, "Modeling of ge wind turbine-generators for grid studies," *GE energy*, vol. 4, pp. 0885–8950, 2010.

[16] U. Annakkage, P. McLaren, E. Dirks, R. Jayasinghe, and A. Parker, "A current transformer model based on the jiles-atherton theory of ferromagnetic hysteresis," *IEEE transactions on power delivery*, vol. 15, no. 1, pp. 57–61, 2002.

[17] R. Reis, F. Lopes, W. Neves, D. Fernandes Jr, and F. A. Neto, "Effects of ccvt stray capacitances on traveling wave-based applications," *Electric Power Systems Research*, vol. 195, p. 107154, 2021.

[18] F. V. Lopes, M. J. Davi, and M. Oleskovicz, "Assessment of traveling wave-based functions in inverter-based resource interconnecting lines," *Electric Power Systems Research*, vol. 223, p. 109578, 2023.

979-8-3315-8138-1